QUAD FLAT NO-LEAD (QFN) DEVICE FAULTY DETECTION USING GABOR WAVELETS

By

Tay Wai Lun

15384

FINAL PROJECT REPORT

Dissertation submitted in partial fulfilment of the requirements for the Bachelor of Engineering (Hons) Electrical and Electronic Engineering

Universiti Teknologi PETRONAS

Bandar Seri Iskandar

31750, Tronoh,

Perak Darul Ridzuan

CERTIFICATION OF APPROVAL

QUAD FLAT NO-LEAD (QFN) DEVICE FAULTY DETECTION USING GABOR WAVELET

By

Tay Wai Lun

15384

A project dissertation submitted to the

Electrical and Electronics Engineering Programme

Universiti Teknologi PETRONAS

in partial fulfilment of the requirement for the

Bachelor of Engineering (Hons) Electrical and Electronics Engineering

Approved by,

_____

Ms. Norashikin Bt. Yahya

Project Supervisor

UNIVERSITI TEKNOLOGI PETRONAS

TRONOH, PERAK

September 2014

CERTIFICATION OF ORIGINALITY

This is to certify that I am responsible for the work submitted in this project, that this original work is my own except as specified in the references and acknowledgements, and that the original work contained herein have not been undertaken or done by unspecified sources of persons.

_____

TAY WAI LUN

Abstract: Computer vision inspection system using image processing algorithms have been utilized by many manufacturing companies as a method of quality control. Since manufacturing industries comprise of many types of products, various image processing algorithms have been developed to suit different type of outputting products. In this paper, we explored Gabor wavelet feature extraction as a method for vision inspection. Unlike conventional vision inspection system which require manual human configuration of inspection algorithms, our experiment uses Gabor wavelets to fractionate the image into distinctive scales and orientations. Through chi-square distance computation, the physical quality of Quad Flan No-Lead (QFN) device can be distinguished by computing the dissimilarity of the test image with the trained database, thus eliminating the weakness of human errors in configuration of vision systems. We performed our algorithm testing using 64 real-world production images obtained from a 0.3 megapixel monochromatic industrial smart vision camera. The images consists a mixture of physically good and defected QFN units. The proposed algorithm achieved 98.46% accuracy rate with the average processing time of 0.457 seconds per image.

Acknowledgement

"If you can read this, thank a teacher"

- Harry S. Truman -

Deriving its ambiguous meaning, "*this*" from the quote above refers to this entire Dissertation Report for my Final Year Project entitled: *Quad Flat No-Lead (QFN) Device Faulty Detection Using Gabor Wavelet.* I am very much grateful to my project supervisor, Ms. Norashikin Yahya who has been a great mentor, consistently shedding more lights on me with utmost patience and Associate Professor Dr. Hisham Hamid, who always have guided me during my difficult times.

Also, there is a need in me to express my sincere gratitude to my parents who gave their undying support towards my dream in pursuit of knowledge. Without them none of these can be achieved.

TABLE OF CONTENTS

LIST OF FIGURES

LIST OF ABBREVIATIONS

QFN – Quad Flat No-Lead

GUI – Graphic User Interface

ROI – Region of Interest

IC – Integrated Circuits

PCB – Printed Circuit Board

FT – Fourier Transform

CHAPTER 1

INTRODUCTION

1.1 Background

1.1.1 *Quality Controls using Vision Inspection System*

Globally, manufacturing industries are relying heavily on computer vision inspection system to perform quality controlling duties. Computer vision inspection systems are replacing manual human inspection simply because automation is more reliable, accurate, lower operating costs as well as it can replace labour shortage problems. The bloom of computer vision inspection system was initiated in the 1990s where fast-consuming products are mass produced and inspections were required to inspect before delivering the final outputting products to the next process.

Computer vision inspection system is performed using a set of image acquiring camera on the production lines to capture images of outputting products. These captured real-time images are fed into the inspection computer and are analyzed by a programmed software whether or not it has surpasses a standard quality value. With sophisticated algorithms chosen and taught to the computer, the result of the image inspection is able to be used to control any automation to prevent defected appearance products to be packaged or to further process.

The dawn of this new technology of utilizing computer vision to perform automation in manufacturing industry has surpasses great amount of milestones. An example of a vision inspection system in pharmaceutical industry is illustrated in Figure 1. Nevertheless, the field of vision inspection has promoted programmers, software engineers as well as scientists to develop more distinctive image processing algorithms to keep up with the designs of ever-changing complexity of manufacturing products.

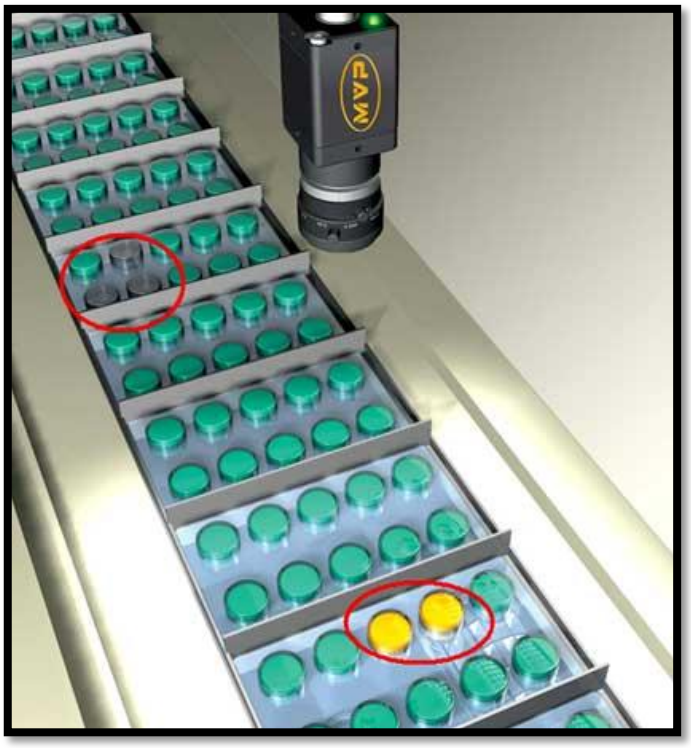

Figure 1: Example of Vision Inspection System in Pharmaceutical Industry

1.1.2 Quad Flat No-lead (QFN)

In semiconductor packaging, Quad Flat No-lead (QFN) devices are one of the highest outputting products in today's manufacturing plants. Figure 2 shows the front and the back view of a QFN device. QFN packages may consist of any type of electrical integrated circuits (IC), be it a Flip-Flop device or mono-stable multi-vibrators. QFNs are famous for their thin features and leadless connection points where they can be soldered onto (Printed Circuit Board) PCBs and forms multiple layered controller boards. Aside from these special features, they use surface-mount technologies, which connect ICs to the surface of PCBs without through-holes. The internal of a QFN consist of one or multiple simple processor (silicon die) which is/are electrically connected by very thin gold wires (1-2 mils in diameter).

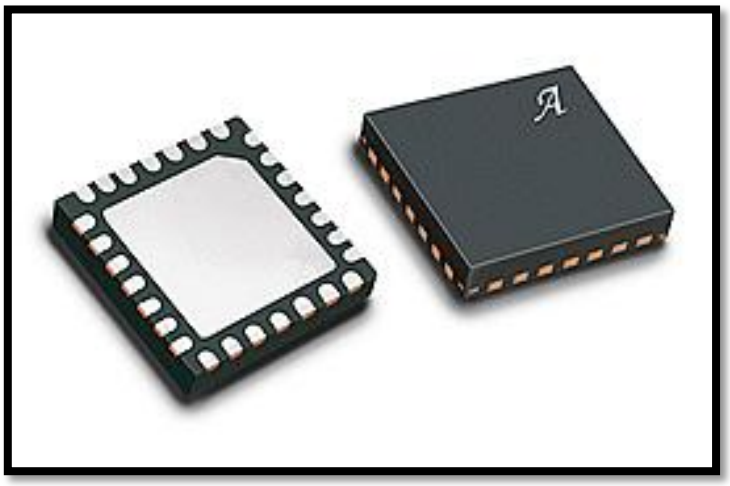

Figure 2: Quad Flat No-Lead Semiconductor

This type of semiconductor package has advantages such as reduced lead inductances, small sized, thin profile and low in weight. Nevertheless, it is an ideal choice for many applications where size, thermal, weight and performance are crucial criteria. With such outstanding semiconductor created, and will be manufacturing all over the world in the future, the need of controlling these outputting devices with minimal human error has to be introduced.

One of the commonly used automatic inspection system in semiconductor machines software is Teledyne Dalsa's iNspect Express. The Graphic User Interface (GUI) for the vision system is shown in Figure 3. In this software, an operator has to manually configure the inspection tool and their region of interests (ROI) in order to perform vision inspections. With the configuration vary from human to human, there may exist variation in the configuration process. Due to this drawback, we proposed a method that will automatically distinguish the physical quality of QFNs without the need of manual human configuration.

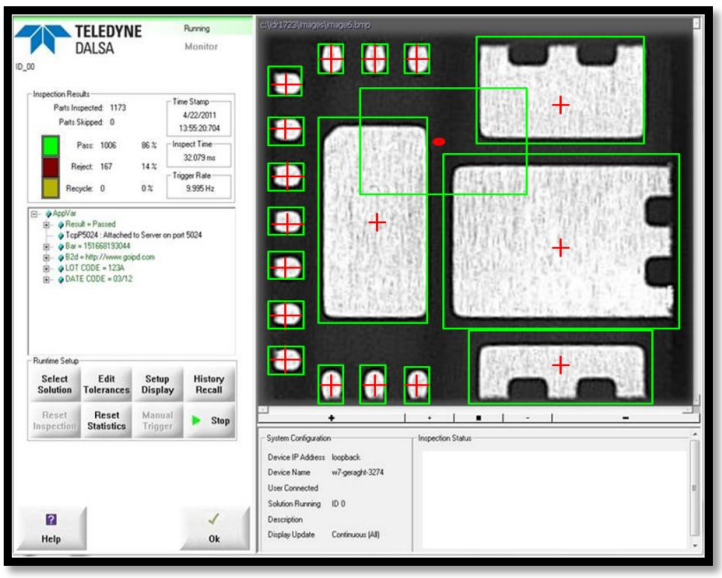

Figure 3: Configuration Interface of Inspection Tools and Region of Interests

1.2 Problem Statement

Technically, in figure 3, multiple layered of inspection algorithms are required to accurately inspect a product. For example, due to minute shifting of location of a QFN, edge detection is used to detect the exact location of the device in an image, and the orientation angle of the product must be precisely identified before further image processing algorithms are configured. The use of manual configuration, at most time, causes the inconsistency of algorithms used, and constant testing had to be experimented to find out the ultimate accurate inspection recipe, and due to that aspect, longer downtime is used to setup a vision inspection system.

1.3 Objective of Project

The objective of this project is to develop a QFN inspection technique using Gabor wavelet for the detection of physically defect units.

1.4 Scope of Study

The scopes of study for this project include:

- Understanding the Gabor wavelet mathematical function and use it as a feature extraction technique.
- Evaluation and implementation of chi-square distance in order to calculate distance between test units and database units
- Development of interface in MATLAB programming to run the both integrated aforementioned algorithms on real-world QFN images.
- To evaluate the inspection algorithm using real-world production images of QFN to obtain the effectiveness of proposed algorithm.

CHAPTER 2

LITERATURE REVIEW AND THEORY

2.1 Gabor Wavelets

Gabor Wavelets is a filter which has the capability of extracting features and captures the spatial characteristics as well as in frequency domain for pattern recognition. The essential characteristic of the wavelet can be applied on images to extract features at particular angles which is useful in extracting the energy of a test QFN image [13], [17].

Gabor Wavelet is commonly used in image processing for their distinctive ability in providing optimal resolution both at time and frequency domains. Due to the fact that the information about time is lost when any analyzing frequency of a given signal is processed through the Fourier Transform into frequency domain, a time-frequency analysis method to represent 1-D signal in time and frequency should be used. Hence, Gabor function has been proven by numerous researches to achieve a representation of both time and frequency domains [2].

Gabor wavelet is optimal both in distortion tolerant feature in texture segmentation and also measuring local spatial frequencies. The mathematical representation of 2D Gabor wavelet is a complex exponential modulated by a Gaussian function defined as shown [3], [5]:

$$\varphi_{u,v}(x,y) = \frac{f_u}{\pi\gamma n} e^{(-(\alpha^2 x'^2 + \beta^2 y'^2))} e^{j2\pi f x'} \quad (1)$$

$$x' = x\cos\theta_v + y\sin\theta_v \quad (2)$$

$$y' = -x\sin\theta_v + y\cos\theta_v \quad (3)$$

where:

f is the central frequency of the sinusoidal plane wave is,

θ is the anti-clockwise rotation of the Gaussian and the plane wave.

The α represents the sharpness of the Gaussian along the major axis parallel to the wave

β is the sharpness of Gaussian along the minor axis perpendicular to the wave.

γ equals to the ratio between the centre frequency and

n equals to the size of the Gaussian envelope.

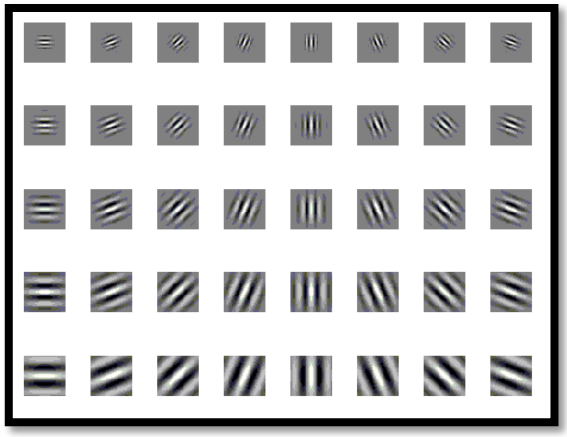

Figure 4: Real Part of Gabor Wavelets at Five Scales and Eight Orientations

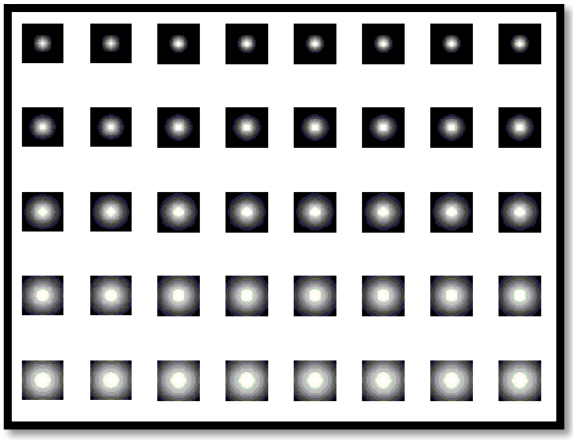

Figure 5: Magnitude Response of Gabor Wavelets with Five Scales and Eight Orientations.

The real parts of 5-scale and 8-orientation Gabor wavelet are shown in Figure 4 and its magnitude responses are given in Figure 5. For computational purpose, the energy extraction is performed by convoluting an input image of QFN and the Gabor wavelet. Let a test image of QFN denote by $Q(x, y)$ and the Gabor wavelet in figure 3 is $\varphi_{u,v}(x, y)$. Thus, the complex convolution of the test images with the wavelets is denoted by the equation [17], [5]:

$$G_{u,v}(x, y) = Q(x, y) * \varphi_{u,v}(x, y) \quad (4)$$

The Fourier Transform (FT) of the original QFN image in Figure 6.1(a) is done to represent the image in frequency domain. The FT image in Figure 6.1(b) is then multiplied with the Gaussian masks angular band at 0° as illustrated in Figure 6.1(c). Note that same scaling is used for all FT results to allow visual representation for comparison purposes.

Similarly, FT filtered images in Figure 6.2(a) represented the result at higher polar radius value. The ripple-type structure of the transformed image can be seen through inverse Fourier Transform of the resultant image in Figure 6.2(b). It is the indication of presence of positive and negative values which should contribute to the energy feature of an image. Thus, the local energies can be computed in Figure 6.2(c) through taking the sum of squares of the resultant image values denoted by the finite-length energy equation below:

$$\sum_{n=0}^{N} |x[n]|^2 \tag{5}$$

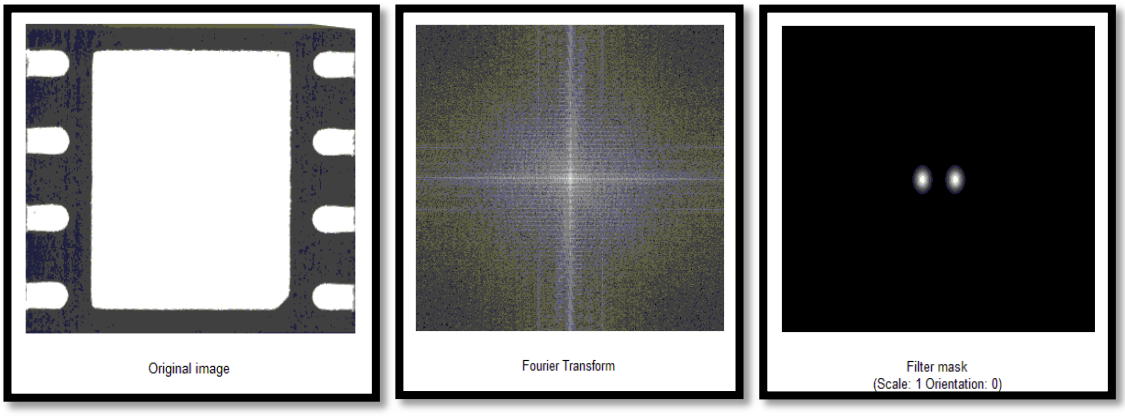

(a) (b) (c)

Figure 6.1: (a) Original Image of Good QFN. (b) The magnitude of its Fourier Transform of Good QFN (for visualisation purpose). (c) Filter mask at scale: 1 orientation: 0

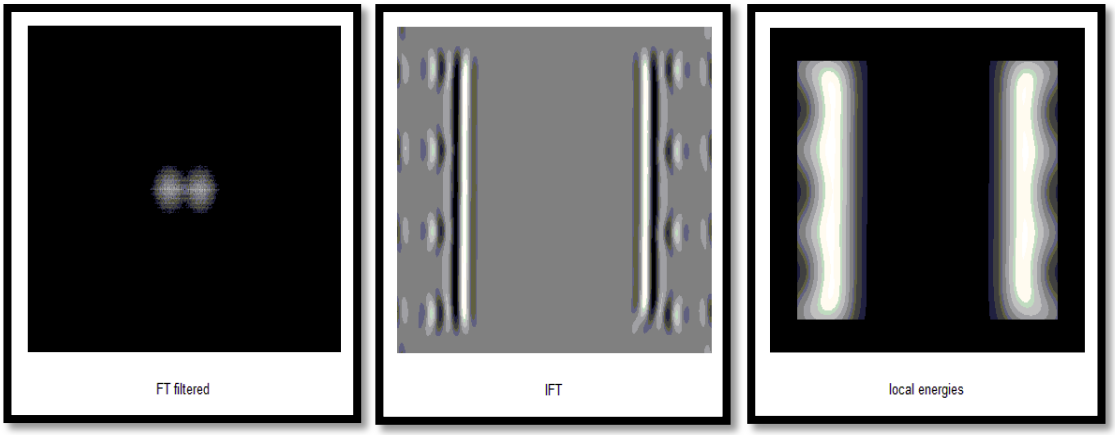

(a) (b) (c)

Figure 6.2: (a) Multiplication with Gaussian masks at 0°. (b) Inverse Fourier Transform (c) Local energy features computed.

Gabor wavelet is able to project orientation selectivity and spatial locality. However, the disadvantage of this method is the non-orthogonal characteristic of Gabor wavelet. This disadvantage would increase the size of any image representation and any other information in the test image itself [14], [5].

2.2 Chi-Square Distance

Chi-square distance function is defined as follows:

$$\chi^2 = \sum_{i=0}^{L} \frac{(v_i - vp_i - 0.5)^2}{vp_i} \quad (6)$$

The value of v_i equals to the frequency of a distance being $i = (0, \dots, L)$, and p_i is probability of the distance being i calculated from the tested probability distribution function.

According to Zhao et. al., to determine threshold, the chi-square distance is used to differentiate two sets of data, in our case, the first Gabor-energized image with the entire array of trained images [19]. The trained images consist of a batch of fifty (50) good unit Gabor-energized feature extracted images. Zhao et. al., also mentioned that in order to perform chi-square distance test, a large number of test images should be made available, which in our case, performed using the aforementioned batch of good QFN production images [19]. The usage of chi-square distance is also supported by which in their 2013 research article encouraged the used of chi-square distance or Kolmogorov-Smirnov distance to match index vectors [15]. This is performed in order to find the maximum threshold value by calculating the dissimilarity between training samples and a test sample, which in our case, a batch of good units and a good unit.

Dagher et. al., research article in face recognition using voting technique, stated that the computation of chi-square distance is a robust distance measure, fast processing algorithm and easy to be implemented [13]. It was chosen as their computation algorithm for the training phase of their research. In our very own training section, the return value of chi-square distance is in term of distance vector between training samples and a test sample.

CHAPTER 3

METHODOLOGY

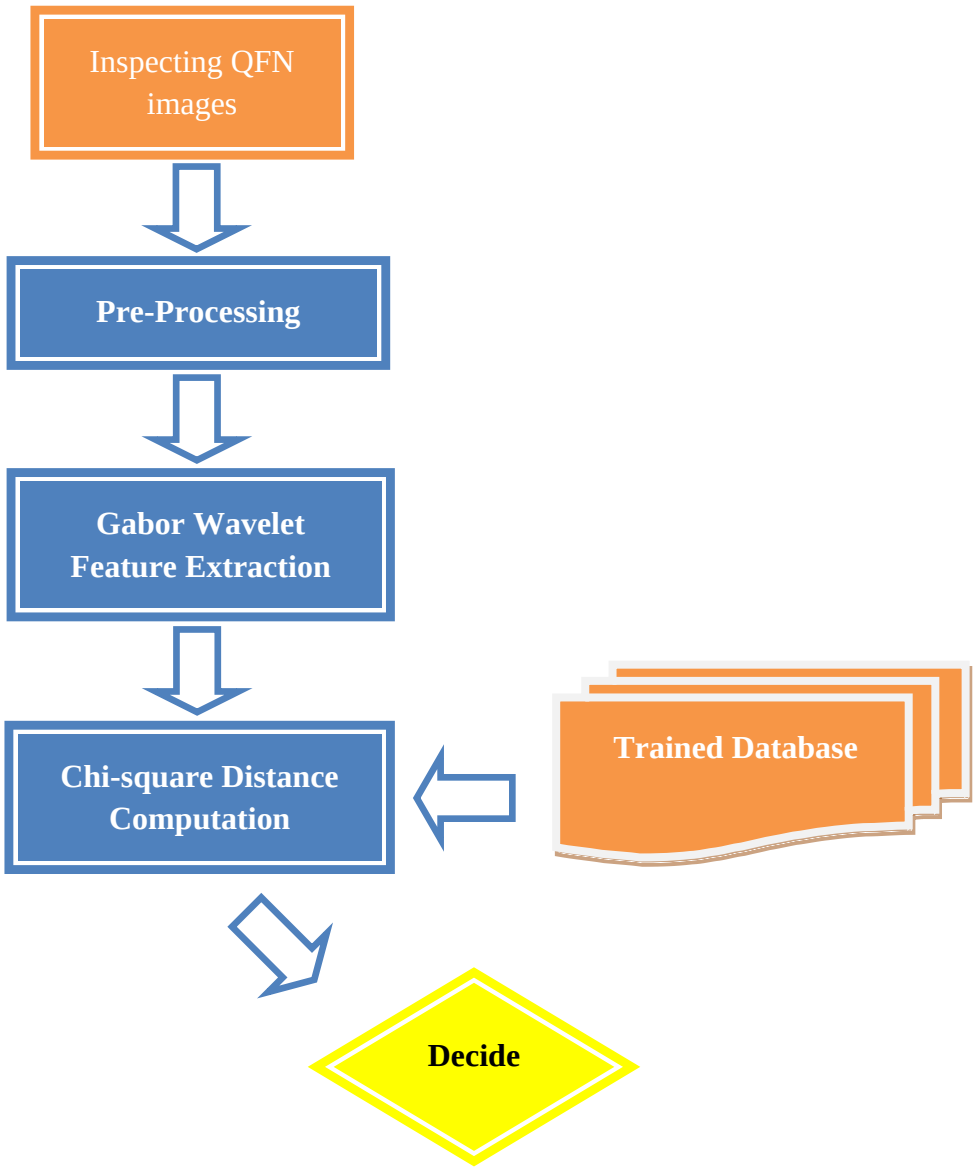

Figure 7: Process flow for Gabor Wavelet Feature Extraction and Chi-square Computation.

3.1 Prior to Image Processing Application

The experiment has been segmented into three stages. The first stage of the project involved data acquisition and pre-processing stage. Samples of real-world production images are acquired from a local semiconductor packaging plant. The sample images consist of good and bad quality units which will be used for training and algorithm testing purposes.

Real-world QFN images from test assembly production line are not appropriate for Gabor wavelets processing and chi-square dissimilarity computation. The test images are captured by a 0.3 monochromatic industrial smart vision camera. These test images shows the bottom pad of the QFN. A sample of a QFN image captured through smart camera is shown in Figure 8.

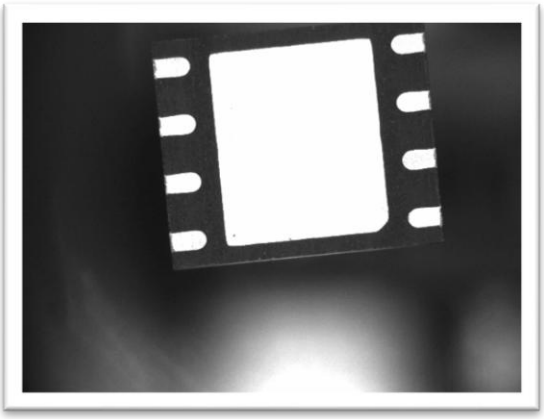

Figure 8: Image of QFN Obtained From Vision Inspection System

The raw image such in Figure 8 are pre-processed prior to Gabor wavelet feature extraction processing. In particular, the image is straightened and background was removed. Notably, the images captured with the QFN appeared to be small in relative to the rest of its image. The images consist of non-interested dark area because of the optics was not properly calibrated accurately to capture the QFN whole. In other words, for all the images captured, there exist large, non-interested region for the Gabor wavelet and chi-square distance to accurately process. Therefore, pre-processing must be done prior to Gabor wavelet feature extraction process by realigning and cropping out the region which are useless for the Gabor wavelet to extract features. Thus, a total of 50 of good units are manually realigned and cropped. A sample of a pre-processed image is shown in Figure 9. These 50 images are used to train the database using Gabor wavelet and chi-square distance.

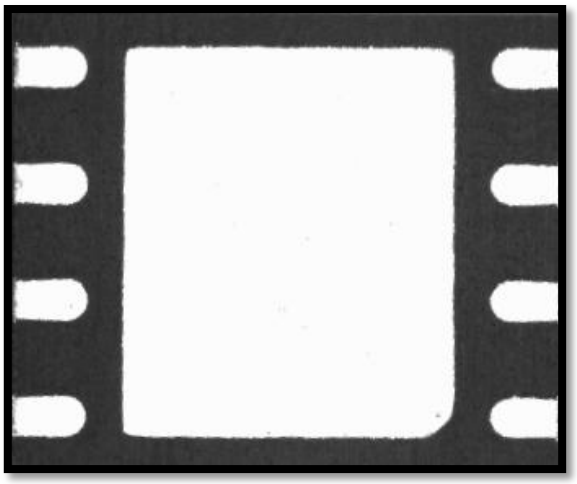

Figure 9: Pre-Processing of Realignment and Cropping

The pre-processing was done with reliable software which does not alter the original image but only straightened and resized accordingly to distinctive features of the image. There were no alteration of the data in the region of interest and the purity of the images is preserved. The Gabor algorithm processes the images in even number of pixels. Thus, the resizing of these pre-processed images has to be cropped into even values.

3.2 Training Phase

3.2.1 Gabor Wavelet Feature Extraction

In the training phase, the processes of Gabor wavelet feature extraction and the chi-square dissimilarity computation is used to establish a database of knowledge. 50 pre-processed test images of QFN devices consist of all good QFN units are classified from T1 to T50. All of the 50 test images will be Gabor feature extracted and form into an array of 50 feature extracted images, the G-array.

3.2.2 Chi-Square Distance Computation

Chi-square dissimilarity computation was performed between the G-array of 50 feature-extracted images and the first feature extracted image. The return values of the chi-square result would be in terms of integer values with each computation yielding 50 results.

$$[T1 \ldots t50] * T1,\ldots,T50$$

Consequently, the subsequent T2 to T50 are chi-square computed with the G-array as well. Therefore, each sets of computation between the G-array and a single test image will yield 50 dissimilarity score. Ultimately, the results returned were 50 dissimilarity values with 50 sets of computations.

3.3 Threshold Setting

After the pre-processing stage and training phase have been performed, the current workspace now contains the returned values of the chi-square dissimilarity computation of 50 Gabor feature-extracted QFN images. The results of each computation of [T1 … T50] * T1 to [T1 … T50] * T50 shows the degree of dissimilarity between the first image with the G-array up to the last image with the G-array. It is understandable that the test images are all good QFN units, thus yielding a very low dissimilarity value.

Consequently, the values of all 50 x 50 sets of computation are generated. With [T1 … T50] * T1 resulting 50 dissimilarity values, and computations were performed from T1 to T50, each computed values generated was averaged to find the mean value of dissimilarity. Therefore, the highest mean dissimilarity value of the computation is used as the threshold limit for later stage of algorithm testing process.

3.4 Algorithm Testing

The final stage of the experiment involved the testing the robustness of the algorithm where the whole integrated algorithm is put to image processing analysis of 64 test QFN production images. A simple interface was created to run the system by feeding the 64 inspection images into the algorithm. Similarly to previous stages, these 64 inspecting images are required for pre-processing of realignment and cropping. The images consist of 50 good units and 14 physically defected units. Figure 10 shows the real-world production images used to test the effectiveness of proposed algorithm.

Recalling the upper limit of threshold value defined during the 'Threshold Setting' stage, the threshold value represents the highest dissimilarity score between good QFN unit and 50 good QFN units. Understandably, if inspecting test images during algorithm testing mode consist of any QFN images which are not similar to the database would yield a very high chi-square value. With high value detected (exceeding the threshold limit), the inspecting image is considered failed.

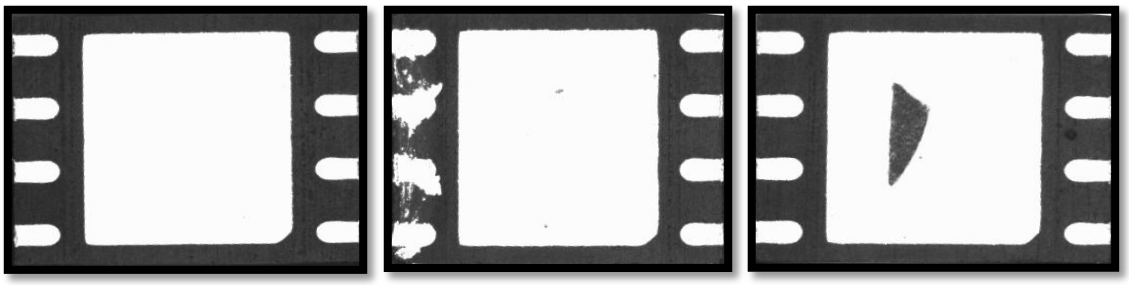

(a) (b) (c)

Figure 10: (a) Good QFN unit. (b) Smeared QFN unit. (c) Contaminated

CHAPTER 4

RESULTS AND DISCUSSION

4.1 Results in Training Phase

Fifty (50) QFN images were used to train the algorithm and form a database of knowledge to demonstrate the robustness and effectiveness of this project. The images of good quality QFNs contain no physical defects and the images were unaltered except the stage of pre-processing of realignment and cropping. Additionally, these images were captured under a consistent illumination with no disturbance of noises.

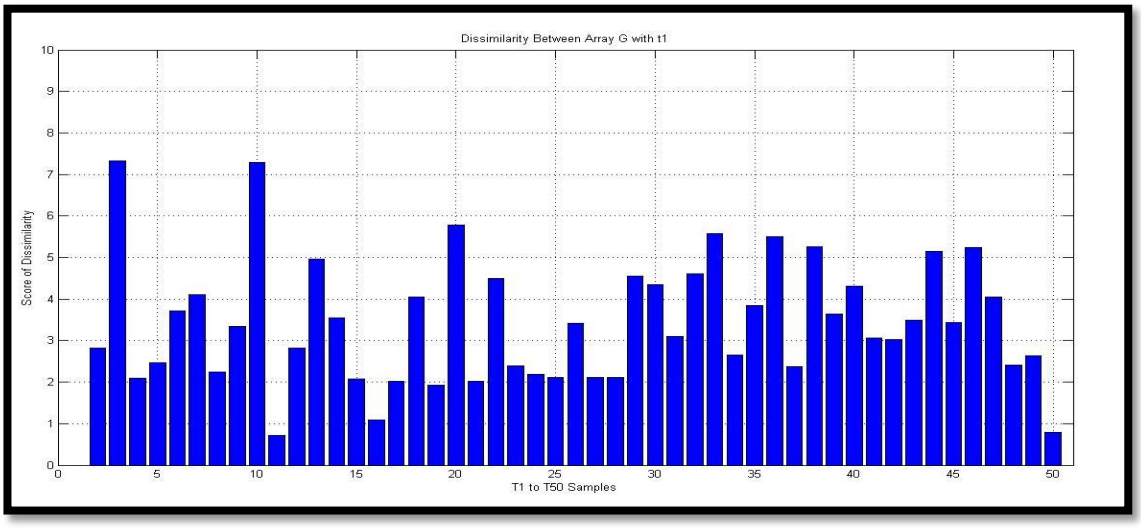

Figure 11: Dissimilarity Values Computed between G-array and `T1`.

Based on the process explanation in previous methodology chapter, figure 11 shows the result of the G-array dissimilarity with the first trained image, [`T1` … `T50`] * `T1`. Note that the G-array consists of good QFN images `T1` to `T50` thus; causing the dissimilarity between the first training image, `T1` and `T1` equals to zero (absolute identical).

Similarly, the G-array was used to compute the chi-square distance for all subsequent training images T2 to T50. Figure 12 and 13 depict the chi-square distance computation result for T2 to T3 with the G-array. Consequently, the values of zero dissimilarity can be seen for all training images from T2 to T50 with the G-array.

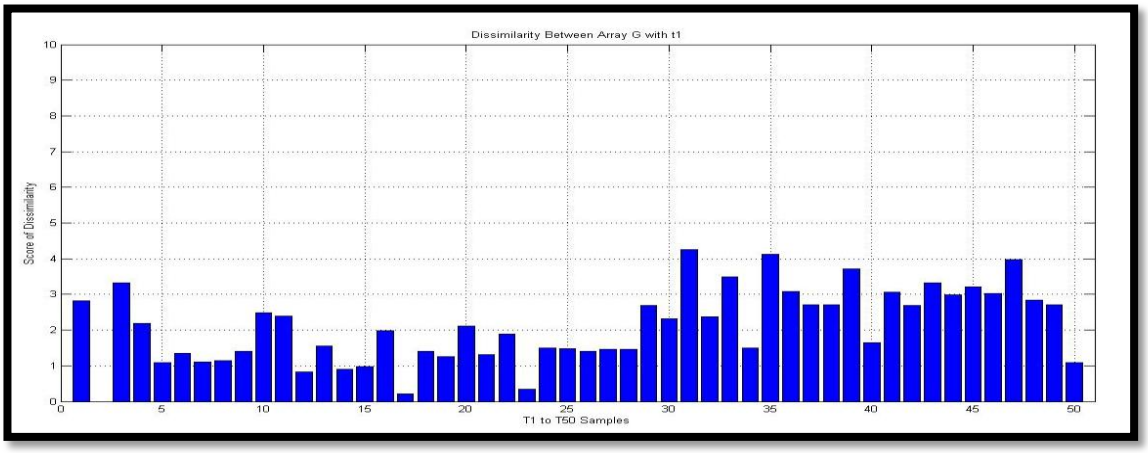

Figure 12: Dissimilarity Values Computed between G-array and T2.

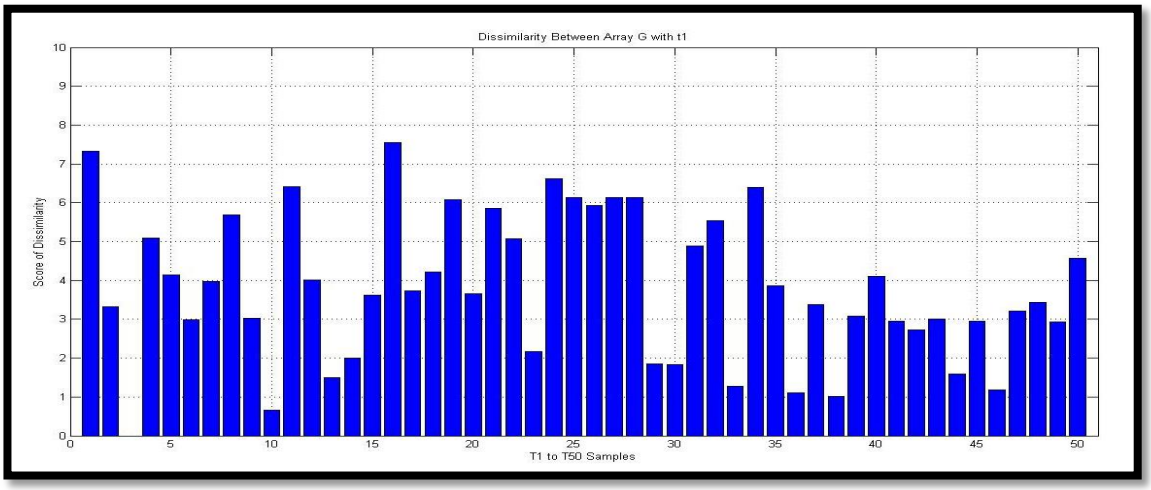

Figure 13: Dissimilarity Values Computed between G-array and T3.

The graphs above represent the dissimilarity values of G-array with each training images. Therefore, with such high data obtained, the mean values of the dissimilarity computation between the G-array and a test image represent intensity of the dissimilarity of the images in the G-array is with the single training image. Taking the average of all 50 trained chi-square distance computed data provide a general overview of how identical these images are with each other. The Figure 14 below shows the mean values of each computation.

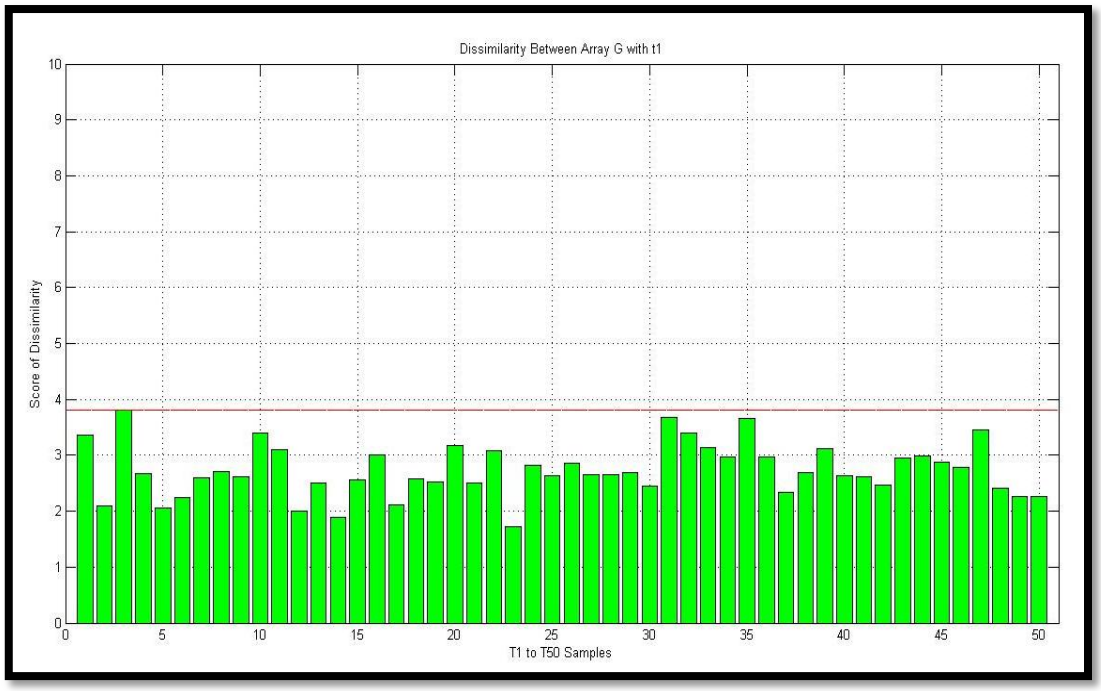

Figure 14: Mean Values of All Chi-Square Computations.

Notably, the red line in Figure 14 above represents the maximum value of dissimilarity between the entire G-array with the test images from `T1` to `T50`. The maximum values computed from the mean chi-square values were 3.8013. This value is used to define the maximum limit (threshold) for algorithm testing. In summary for the training phase, an inspecting image may score lower or equal to this value in order to categorize as a physical appearance passes quality inspection. Any values scored higher than the threshold value will be considered as physically failed inspection units.

4.2 Results in Algorithm Testing

In the algorithm testing stage, a total of 64 production QFN images were inspected using the algorithm. Out of the 64 images, 50 are good QFN units and 14 consist of defected QFN units. The defected units consist of smeared pads, contamination, missing lead, wide pitched and scratched pads. Shown in Figure 15 are a good unit and examples of defected units.

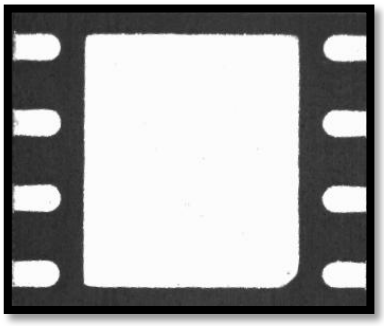

Figure 15: Good QFN unit.

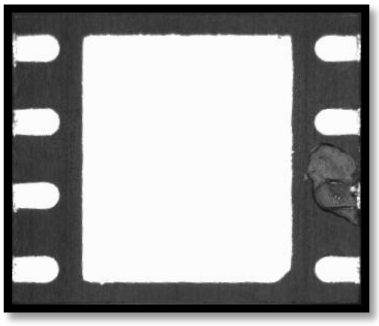

Figure 16: Missing lead defect

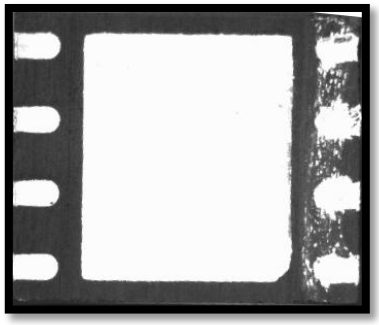

Figure 17: Smeared QFN unit.

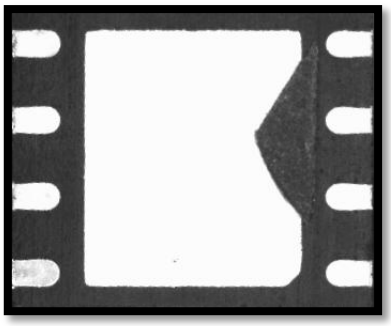

Figure 18: Foreign Material

A simple interface was created to inject the 64 production images into Gabor wavelet feature extraction. Next, the inspecting Gabor energized image was chi-square computed with the G-array to find the dissimilarity value.

Out of the 50 good QFN units, all were inspected passed quality. Meanwhile, for the 14 defected units, 13 were inspected as failed physical quality with 1 escapee (1 unit failed to be detected by the algorithm). The possible reason of the escapee which failed to be detected by the algorithm could mainly due to the nature of the defect itself. The escapee was a scratched pad escapee where the intensity of the scratches were too minimal to be explicitly illustrate by the illumination technique of the vision inspection camera module.

Figure 19 illustrate the graphic representation of algorithm testing. The sample of tests images were the aforementioned 64 production images of QFN devices. Images 1 to 50 are good units, and 51 to 64 are defected units. Dissimilarity values were obtained through the computation using chi-square distance. Similarly, the red line indicates where there threshold value was defined. The threshold value act as the limit for the inspecting test image where none inspecting test images should yield any score higher than the defined threshold. Any images inspected with dissimilarity values higher than the threshold are considered physically defected units.

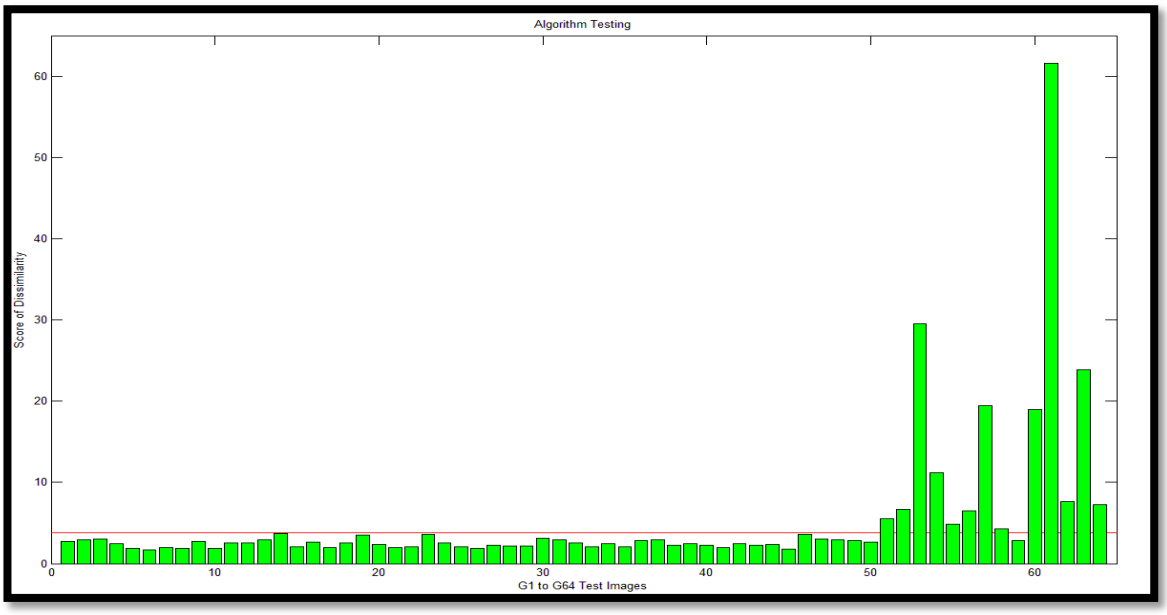

Figure 19: Algorithm Testing Result for Test Images G1 – G64

Note the first 50 good QFN images did not surpass the threshold limit because the dissimilarity values computed after Gabor wavelet feature extraction were lower than the threshold (good QFN units). Consequently, the defected units starting from image 51 exceeded the threshold limit. Image 59 was the aforementioned scratch escapee which did not exceed the threshold limit (failed to be detected by the algorithm). Ultimately, 63 out of the 64 were correctly inspected thus; yielding the accuracy of the algorithm at 98.43% accurate, with the average processing time of the algorithm at 0.457 seconds per image.

4.3 Discussion

The algorithm was integrated in a way which utilizes a batch of good units to act as a database of knowledge. With the training images processed with Gabor wavelet and chi-square distance computed, it is safe to say that the dissimilarity values obtained from database are reliable enough to find a maximum limit as the threshold. With such threshold value established, vision inspection can be performed in comparison to the threshold value practically without the need of human configuration. Through this method, we may have totally eliminated human error in vision inspection system configuration.

The database used for the algorithm testing was limited to 50 Gabor energized images. Practically, in real-world application, this algorithm system is designed in a way which can be trained using large amount of good quality unit images. Only with larger number of training images stored in the database, the system would yield higher reliability. Additionally, in our experiment of testing the algorithm, there were only 64 production images used to be tested, causing each inspecting images yield bigger fraction of percentage in the accuracy calculation. Ideally, if sufficient amount of images can be obtained, the percentage of the accuracy may yield at a higher rate.

Chapter 5

Recommendation and Conclusion

Recommendation

In aforementioned concern about the percentage accuracy, certain industry has very strict regulations in using newly proposed vision inspection algorithms. For instance, semiconductor vision inspection system must have the accuracy rate of 99.99%. Whereas other industry regulation permits lower accuracy rates, depending to the types of products. Despite a very positive result obtained, the progress of this project has limited amount of test images for algorithm testing stage. Therefore, as part of the recommendation, more data of images are required to ascertain the true accuracy rate of this algorithm and clearly define the effectiveness of this algorithm before implementation of the proposed algorithm in vision inspection system.

Moreover, the processing time of the algorithm using MATLAB programming yield 0.457 seconds per images. The time consumed to process an image and return a pass/fail result has taken too long. In real-world application for QFN devices, there are vision inspection modules which can process images as fast as 10 milliseconds per image. Due to this speed, higher productions of QFNs are able to be outputted from the plant. Therefore, to ascertain this experiment be a competent algorithm, the recommendation to tackle this situation is to refine the algorithm or otherwise, the entire algorithm has to be programmed in another type of programming platform such as OpenCV or C++. By doing so, the processing time of the algorithm can be enhanced thus, does not outputting quantities of prospective industries.

Conclusion

In this paper, we have presented an alternative method of vision inspection algorithm to inspect the physical quality of QFN devices in semiconductor packaging industry. By using Gabor wavelet to extract the features of good quality QFN devices, chi-square distance is then used to compute the dissimilarity of the images to form a database. Through this method, a vision inspection system may not require human configuration. The robustness and the effectiveness of the method have been tested through experiments using real-world vision inspection images. Our proposed inspection algorithm using Gabor wavelet and chi-square distance algorithms obtained competent outcome with the accuracy of 98.43%. Additionally, an average of 0.457 seconds processing time for an image was achieved in our experiment. We too, assured the consistency of our result, using a batch of good QFN images to train the algorithm; however, this algorithm is still subjected to various unforeseen limitations where it could yield different result and values under different types of images or products. Therefore, to fully comprehend the limitations of this algorithm, in depth experiments has to be performed on other sets of images to fully comprehend the behaviour of this algorithm. In summary, Gabor wavelet and chi-square distance computation may form a database of knowledge to compare test images physical quality and may be used for similar experiments.

References

[1] Kepenekci, B. (2001). *Face recognition using gabor wavelet transform* (Doctoral dissertation, MIDDLE EAST TECHNICAL UNIVERSITY).

[2] Serrano, Á., de Diego, I. M., Conde, C., & Cabello, E. (2010). Recent advances in face biometrics with Gabor wavelets: A review. *Pattern Recognition Letters*,*31*(5), 372-381.

[3] Choi, W. P., Tse, S. H., Wong, K. W., & Lam, K. M. (2008). Simplified Gabor wavelets for human face recognition. *Pattern Recognition*, *41*(3), 1186-1199.

[4] Shen, L., Bai, L., & Fairhurst, M. (2007). Gabor wavelets and general discriminant analysis for face identification and verification. *Image and Vision Computing*, *25*(5), 553-563.

[5] Struc, V., Gajsek, R., & Pavešić, N. (2009, September). Principal Gabor filters for face recognition. In *Biometrics: Theory, Applications, and Systems, 2009. BTAS'09. IEEE 3rd International Conference on* (pp. 1-6). IEEE.

[6] SHEN, L. L., & JI, Z. (2009). Gabor wavelet selection and SVM classification for object recognition. *Acta Automatica Sinica*, *35*(4), 350-355.

[7] Liu, C., & Wechsler, H. (2002). Gabor feature based classification using the enhanced fisher linear discriminant model for face recognition. *Image processing, IEEE Transactions on*, *11*(4), 467-476.

[8] Bařina, D. (2011). Gabor Wavelets in Image Processing}. In *Proceedings of the 17th Conference STUDENT EEICT 2011}* (pp. 522-526). Brno University of Technology}.

[9] Lee, T. S. (1996). Image representation using 2D Gabor wavelets. *Pattern Analysis and Machine Intelligence, IEEE Transactions on*, *18*(10), 959-971.

[10] Pichler, O., Teuner, A., & Hosticka, B. J. (1996). A comparison of texture feature extraction using adaptive Gabor filtering, pyramidal and tree structured wavelet transforms. *Pattern Recognition*, *29*(5), 733-742.

[11] Shen, L., Wu, W., Jia, S., & Guo, Z. (2014, May). Coding 3D Gabor Features for Hyperspectral Palmprint Recognition. In *Medical Biometrics (ICMB), 2014 International Conference on* (pp. 169-173). IEEE.

[12] Zheng, Q., Lu, Z., Feng, Q., Ma, J., Yang, W., Chen, C., & Chen, W. (2013). Adaptive Segmentation of Vertebral Bodies from Sagittal MR Images

Based on Local Spatial Information and Gaussian Weighted Chi-Square Distance. *Journal of digital imaging*, *26*(3), 578-593.

[13] Dagher, I., Hassanieh, J., & Younes, A. (2013, August). Face recognition using voting technique for the Gabor and LDP features. In *Neural Networks (IJCNN), The 2013 International Joint Conference on* (pp. 1-6). IEEE.

[14] Zuñiga, A. G., Florindo, J. B., & Bruno, O. M. (2014). Gabor wavelets combined with volumetric fractal dimension applied to texture analysis. *Pattern Recognition Letters*, *36*, 135-143.

[15] Moghaddam, H. A., & Dehaji, M. N. (2013). Enhanced Gabor wavelet correlogram feature for image indexing and retrieval. *Pattern Analysis and Applications*, *16*(2), 163-177.

[16] Guo, J. M., Prasetyo, H., & Wong, K. (2014). Vehicle Verification Using Gabor Filter Magnitude with Gamma Distribution Modeling. *Signal Processing Letters, IEEE*, *21*(5), 600-604.

[17] Abdulrahman, M., Gwadabe, T. R., Abdu, F. J., & Eleyan, A. (2014, April). Gabor wavelet transform based facial expression recognition using PCA and LBP. In *Signal Processing and Communications Applications Conference (SIU), 2014 22nd* (pp. 2265-2268). IEEE.

[18] Cho, H., Roberts, R., Jung, B., Choi, O., & Moon, S. (2014). An Efficient Hybrid Face Recognition Algorithm Using PCA and GABOR Wavelets.*International Journal of Advanced Robotic Systems*, *11*(59), 1-8.

[19] Zhao, Y., Wang, S., Zhang, X., & Yao, H. (2013). Robust hashing for image authentication using Zernike moments and local features. *Information Forensics and Security, IEEE Transactions on*, *8*(1), 55-63.

Appendix

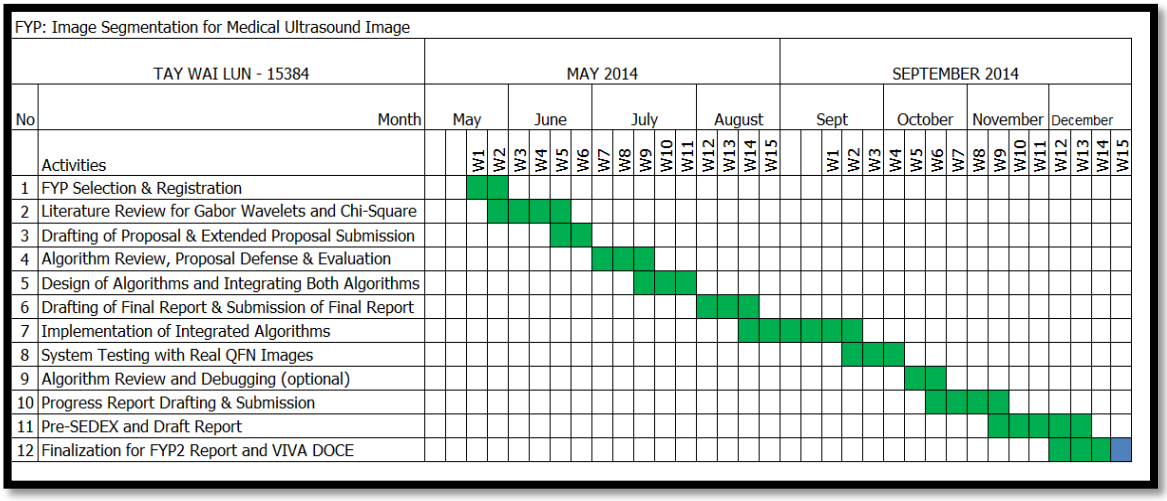

Gantt Chart of FYP